

# THE ENVIRONMENTAL IMPACT OF COLLISIONS WITH LARGE SPACE STRUCTURES: THE CASE OF SOLAR POWER SATELLITES

Pietro De Marchi<sup>(1)</sup>, James Campbell<sup>(2)</sup>, Yirui Wang<sup>(3)</sup>, and Massimiliano Vasile<sup>(3)</sup>

<sup>(1)</sup>*Aerospace Centre of Excellence, University of Strathclyde, Glasgow, UK, Email: pietro.de-marchi@strath.ac.uk*

<sup>(2)</sup>*Brunel University of London, London, UK*

<sup>(3)</sup>*Aerospace Centre of Excellence, University of Strathclyde, Glasgow, UK*

## ABSTRACT

This paper presents the initial steps toward developing a dedicated pipeline for modeling the collision and breakup of large space structures, with a particular focus on Solar Power Satellites (SPS) in Low-Earth Orbit (LEO) and Geosynchronous Orbit (GEO). In the last decades, interest in assessing the advantages and feasibility of deploying SPS in orbit has grown significantly—alongside concerns about the potential risks they pose due to their important size. However, very little research has examined in detail the actual effects these structures could have in terms of collisions and debris generation. The ultimate goal of this research is to develop an accurate yet computationally efficient method for estimating the consequences of impacts involving large space structures, ranging from minor to catastrophic collisions. This approach will enable seamless integration into space environment evolutionary models (such as NESSY or MOCAT), ensuring a more comprehensive assessment of their long-term impact on the space environment. When considering collisions between large space structures and objects ranging from sub-millimetre fragments to geostationary satellites' size, the current NASA Standard Breakup Model (SBM) may be insufficient for accurately capturing the resulting fragment distribution. This is primarily because it usually overestimates smaller debris (on the millimetre scale) and is not designed to account for very large structures. In the existing literature, the effects of hypervelocity impacts are typically studied in detail through experimental collision tests in physical facilities or numerical simulations using Smoothed Particle Hydrodynamics (SPH) or Finite Element Method (FEM) analysis. These approaches are however computationally expensive and inadequate for the integration of algorithms. On the other side, semi-empirical models allow to provide estimates based on real experiment data and better generalise about different scenarios. This research reports the first steps towards developing a semi/analytical based breakup model specifically tailored for large space structures with a focus on SPSs.

Keywords: Solar Power Satellites; Fragments; Standard Breakup Model.

## 1. INTRODUCTION

Space-Based Solar Power (SBSP) technology has been investigated since the 1970s, while a concrete commercial interest has grown just in the last decade, because of the increasing concerns about "green" energy production on Earth. Because of the complexity and high costs of such missions, only a few concepts have been inspected in detail. In GEO orbit one of the most important is the SPS Alpha [7] concept, by NASA (declared power delivered  $\approx 1$  GW). Similar to this one, always for GEO orbit, IECL and Space Solar are working on CASSIOPeiA (Constant Aperture, Solid-State, Integrated, Orbital Phased Array), derived from the original concept HESPeruS (Highly Elliptical Solar Power Satellite [11], declared power delivered more than 1 GW); an idea of I. Cash (at present chief architect at Space Solar). Both concepts aim to converge solar rays with huge collectors and transfer then the energy back to Earth. The first real mission demonstrating the transfer of energy to the planet is the Caltech experiment: the Space Solar Power Demonstrator (SSPD-1)[6] launched in January 2023. A different concept instead is the constellation of LEO reflectors, conceived by ESA and Thales Alenia Space (SOLARIS project): SBSP (Space-Based Solar Power) [12]. Figure 1 shows the ESA reflector's architecture. It is made of a composite membrane ( $\approx 1$ km in diameter and just 4 to 8  $\mu$ m thick) stretched and kept in place by a circular truss ring, while the whole structure is balanced by a central truss mast ( $\approx 564$  m). This concept is intended to be inserted into a down-dusk Sun-synchronous orbit (SSO) at approximately 890 km altitude. Figure 2 instead reports a schematic representation of the CASSIOPeiA concept. The height of the whole structure is  $\approx 3$  km (reflectors are about 2 km in diameter).

Current literature studies for these architectures are mainly focused on commissioning, assembly, power budget and orbital control analyses; but very poor literature covers the impact of such huge structures in terms of collision risk and fragmentation modelling for these scenarios. Because of the huge dimensions of such missions, the traditional approaches could be not optimal for these structures; for example in the case of the LEO reflector where the thickness of the membrane is very differ-

ent from the dimensions of the other components. Furthermore, the LEO environment is highly populated with a growing density of both big objects and small debris (ESA Annual Space Environment report [14] of 2024), that if impacting could result in very different consequences on the structure depending on the component involved. In GEO the collision risk is not that critical but the huge cross-sectional areas of the reflectors and the central helix of CASSIOPeiA increases consistently the risk due to small fragments and micro-meteoroids, which over time could erode consistently some parts of the structure. The main studies analysing the main consequences of the collision effects on SPS are the following. The Thales Alenia technical report [12] in 2023 inspects mainly the collision frequency with small fragments with the LEO reflector, estimating to total amount of cumulated collisions with the membrane. Gordon and McInnes [28], along with the SOLSPACE project, inspect the end-of-life aspects of the LEO reflector concept underlining the main constraints imposed by ESA on collision avoidance concerning major objects and citing the work of Lourens et al. about the qualitative estimate of consequences of impacts with thin membranes as one of solar sails [26]. Regarding instead the GEO scenario (e.g. CASSIOPeiA), no studies have specifically focused on the SPS concept regarding the collision effects, but consequences could be deduced by reviewing the different analyses reported about sphere-wall tests for different impact velocities.

This paper's objective is to present the first steps towards a dedicated pipeline to adequately estimate the consequences of impacts (both local and catastrophic events) involving different parts of a generic SPS on the rest of the space environment. The main challenge in the case of SPSs is defining a model capable of generalizing the analysis to any different typical component of the SPS not losing the accuracy in the phenomena description. SPS components can vary between a few microns in thickness up to a meter (as will be discussed later). The other most important characteristic of this pipeline is to be computationally efficient to be incorporated inside an evolutionary model for the space environment such as NESSY. NESSY (NETwork model for Space SustainabilY) [20] is the tool developed at the Aerospace Centre of Excellence of Strathclyde University that allows a prediction of the evolution of the space environment over time, based on the network theory. At the moment the breakup model employed inside NESSY is the NASA SBM, but to better account for the SPS presence in space, also this new pipeline is going to be integrated.

## 2. BREAKUP MODEL FOR THE SPS USE CASE.

Fragmentation modelling has been largely investigated in literature for space applications through different approaches. Many impact experiments have been investigated, most of them focused on aluminium and carbon-fibre composite plates impacted by spherical impactors. These experiments provide a detailed idea of the consequence of the impact (perforation, structure deforma-

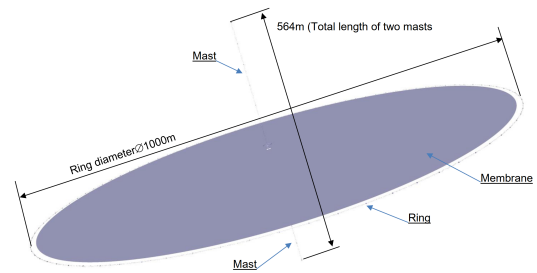


Figure 1. Schematic architecture of a single reflector of the concept studied by ESA [12].

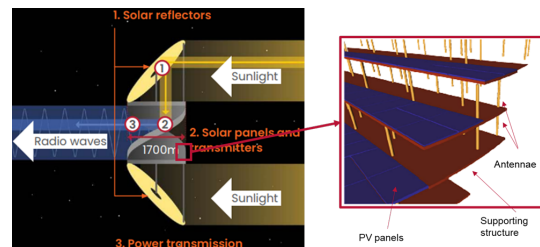


Figure 2. Overview of the CASSIOPeiA concept [11], designed by Space Solar.

tion and shape of the debris cloud produced) with different initial conditions (e.g. different  $t/D$  ratios, where  $t$  is the plate thickness and  $D$  is the impactor diameter, and initial speed). Between the most relevant for the present research, there are the experiments presented by Piekutowsky [22], those by Verma and Dhote [5] and by Nishida [32], [31]. Other major tests involving bigger structures are SOCIT [2] and DebrisSat [4], these have been considered also in the development of the NASA breakup model. These experiments, and many others, have been essential to help in the development of the so-called empirical and semi-empirical breakup models. The most famous empirical model is the NASA Standard Breakup Model (NSBM) [9], developed initially in the 1990s, providing fragments mass, velocity, area-to-mass, and characteristic length distributions derived from empirical data available. On the other hand, semi-empirical models combine mass, momentum, and energy conservation principles with empirically derived relationships. They are based on conservation laws to constrain empirical results, making predictions consistent. These aspects make empirical and semi-empirical models computationally efficient and useful when detailed information about objects involved in the impact is not available or there is a necessity to make the model as much versatile as possible. The most known semi-empirical model-based tools are FAST [33] and IMPACT [3]. These two tools have similar pipelines and derive mass, size (or characteristic length), area-to-mass, and delta-velocity distribution of fragments. Between the two IMPACT relies more heavily on empirical models and data. Another reference is the CST model developed at the University of Padova [27], this model combines different semi-empirical techniques coming from both IMPACT and FAST together with a

computer graphic approach based on the Voronoi pattern, to relate the total number of fragments with their major dimension distribution. Many other researches have inspected the consequences of collisions in space employing numerical simulations such as SPH (Smoothed Particles Hydrodynamics simulation) or FEM (Finite Elements Method) analyses [[17], [18], [24]]. These approaches are ideal for inspecting in detail the behaviour of the collision and having an idea of the shape of the clouds of debris produced. The main limitation of these approaches is that they are computationally expensive, and cannot be included at runtime in other algorithms.

Of all the previous techniques the one selected to model the case of SPS breakup modelling is the semi-empirical approach. SPS structures present a variety of different subcomponents (different in shape and material), meaning a consequent large variety of possible collision scenarios. Semi-empirical approaches allow to cover a wide range of collision scenarios (different types of impactor and target coupling) providing a very good level of precision. However, since the semi-empirical approach strongly depends on the variety of empirical laws available to represent different scenarios, it is necessary to combine this empirical formulation with an algorithm capable of bridging the gap between the different impact conditions considered. This module can be for example an ML (Machine Learning) based algorithm trained on the test data derived from the empirical laws for different scenarios: the initial condition of the fragments cloud after the breakup (number, size, mass and velocity distributions). A more detailed description of the pipeline is described in the next chapters.

### 3. LEO AND GEO POSSIBLE IMPACT SCENARIOS INVOLVING SPS.

In order to define the breakup modelling pipeline for the SPS it is essential to identify in detail all the possible collision scenarios involving the solar power satellites in both LEO and GEO regimes. To do that three main aspects need to be considered: the impactor population, the SPS characteristic components and the velocities involved in the collisions. The first aspect is the identification of all the different impactors that could be involved in collisions with the SPS. Both LEO and GEO SPSs should include collision avoidance strategy and manoeuvres capability for the trackable objects (with average diameters bigger than 5-10cm in LEO orbit and 10cm in GEO orbit). However, because of the huge dimensions of the structures of the SPSs and the consequent relatively elevated risk of collision, especially in the LEO region, it is useful to consider eventual collision scenarios also with major objects, and the related long-term effects. More important is instead to inspect the impact consequences with small fragments (average diameter between 1mm and 10cm). In Figures 3 the distribution of the average diameter of respectively LEO and GEO populations of major objects in 2023 is reported, combining the SatCat [23] and ESA DISCOS [8] databases. In Figure 4 instead

the distribution of small fragments is reported for both regimes. These plots suggest that in LEO the biggest dimension for LEO objects is generally about a few meters, apart from the space station and some upper stages. In GEO instead many platforms and upper stages exceed the 10m.

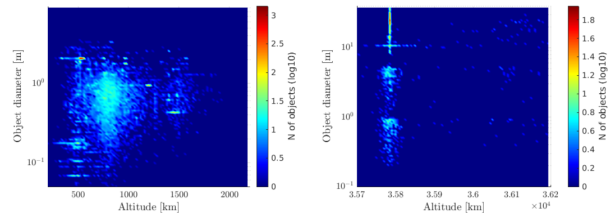


Figure 3. Distribution of the LEO and GEO objects through altitudes and major diameter (objects from ESA DISCOS and SatCat, objects bigger than 10 cm).

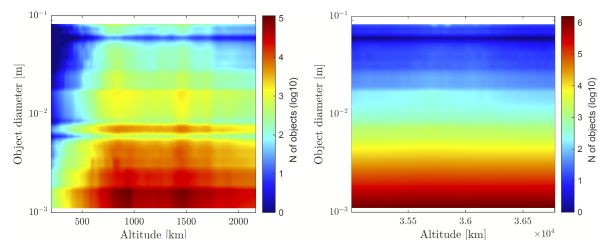


Figure 4. Distribution of the LEO and GEO small fragments through altitudes and major diameter (objects from ESA MASTER, objects between 1 mm and 10 cm).

In LEO as shown by Rossi [25] the collision velocity, depending on the impact angle, shows an average value of  $9.7 \text{ km/s}$ , having minimum values around a few  $\text{km/s}$  and a maximum between  $12$  and  $15 \text{ km/s}$ . In the GEO regime instead, impact velocities are lower, and should be on average about  $800 \text{ m/s}$  [34], with maximum values about  $5 \text{ km/s}$  considering crossing objects like micrometeoroids (slightly higher average for GTO, around  $2 \text{ km/s}$ ). Considering that impacts cover a range between hypervelocity and sub-hypervelocity regimes, between both LEO and GEO. In the case of hypervelocity impact, complex phenomena can lead to pulverization and fusion of the material (depending on peculiar physical properties).

The last important aspect to consider for the modelling of the breakup estimate is the variety of the different possible characteristics of the SPS structures. Table 1 summarizes the different structural types that could be found in different SPS architectures. This wants to summarize the real variety of structure characteristics, considering the most common structures present in SPSs platforms. The table shows that in GEO platforms the maximum thickness could be in some cases higher than the LEO ones, or in general more massive.

This table has been defined from the data of the main mission concept conceived in the last decades (mainly [11], [12], [36], [37], [38], [39]).

Table 1. Identification of the main constitutive objects for LEO and GEO main SPS platforms. Materials: CF = carbon fibre / PEEK / KAPTON, Al = aluminium, FG = fibreglass.  $t$  is the thickness of the structural component.

Orbit regime	Component type	Shape	$t$ range [m]	Material
LEO	Truss structures	modular cylindrical	$10^{-3} - 10^{-2}$	CF
	Membrane	thin plate	$10^{-6} - 10^{-3}$	CF
	Structural layers	thin/thick plate	$10^{-3} - 10^{-2}$	AL, CF
	Solar panels	thin/thick plate	$10^{-3} - 10^{-2}$	Al, FG
GEO	Truss structures	modular cylindrical	$10^{-3} - 10^{-2}$	CF
	Reflector panels	thick plate	$10^{-2} - 10^0$	CF, Al
	Reflective mirrors	thin/thick plate	$10^{-3} - 10^{-1}$	CF, FG
	Structural layers	thick plate	$10^{-3} - 10^{-1}$	Al
	Solar panels	thin/thick plate	$10^{-3} - 10^{-2}$	Al, FG

Previous studies with NESSY [21] show that the average number of collisions with small populations for the LEO reflector is around  $2 \times 10^3$  per year. While in GEO, for CASSIOPeIA the average number of collisions with small fragments and micrometeoroids is about  $2 \times 10^2$ . Considering the worst-case scenario instead of not being capable of performing collision avoidance manoeuvres, collisions with major objects are estimated at 6 potential collisions per year, with NESSY. This proves the fact that the great majority of collisions with the SPSs in both LEO and GEO involve small fragments or minor impacts, not generating huge amounts of fragments bigger than 1mm but still happening very frequently during the SPS life.

The main considerations done in this paragraph are essential for the definition of the breakup model pipeline shown in the next chapter, mainly from the point of view of which type of empirical model is considered, mainly depending on the thickness of the target and dimension of the impactor, or the material of the objects.

#### 4. A MODULAR PIPELINE FOR SPS TAILORED BREAKUP MODELLING.

The current version of the NESSY evolutionary model [20] [21] includes both trackable (objects up to 10cm in major diameter) and untrackable objects (between 1mm and 10cm in major dimension). NESSY is an evolutionary model based on the network theory, which includes five object species: payloads, upper stages, non-maneuvrable objects, fragments and solar power satellites (characteristics similar to those of the payload but kept separated because of the peculiar dimension characteristics and mission profile). Collision consequences between all the objects are at present estimated through the NASA SBM, modifying the minimum dimension threshold according to the minimum dimension treated inside the network itself. The class of solar power satellite is treated slightly differently from the other nodes. A classical node (defined as the space regime between an altitude

and inclination ranges) in NESSY is characterised by the following average characteristics: mass, cross-sectional area, and major dimension. These values are used for both the decay computations and the collision computations (inside the SBM). For the SPS instead the same approach cannot be used, because of the huge structure and then huge mass involved. Depending on the different impactor a fraction of the whole SPS structure is selected.

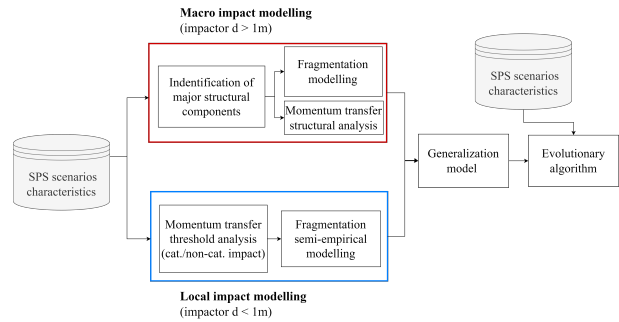


Figure 5. Fragmentation modelling pipeline for SPS.  $*d$  is the major dimension of the objects involved in the impact with SPS.

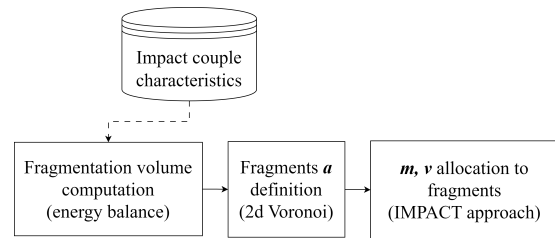


Figure 6. Focus on the local damage impact analysis, as part of the bigger pipeline.

The whole pipeline to model collision and breakup for the SPS is pictured in Figure 5. The flow represented in this scheme pictures the entire approach, while the module that effectively would run inside NESSY is the so-called, "Generalization model", which consists of an ML-based

(Machine Learning) algorithm that will be trained over the outcome of the first part of the pipeline: the distribution of the fragments (in terms of size, mass and velocity) generated by an impact between a generic object and an SPS. The results of the entire pipeline and the outcome of the ML simulations however are not presented in this paper but will be included in the next publications. The selection of the subcomponent of the SPS impacted is done inside NESSY based on the probability distributions of each substructure (e.g. substructures defined in the previous chapter) computed in the same way as done in [21].

To generate the fragmentation data for the ML algorithm two approaches are considered: one "macro impact" approach and one "local impact" approach. Once the impact couple (impactor and target) is defined, depending on the major dimension of the impactor one of the two analyses is considered. For an impactor smaller than 1m in major dimension, the local analysis is selected for the SPS impacted. The local analysis inspects first of all the momentum transfer involved in the impact and defines the fraction of the volume (for both impactor and target) involved considering the impact as happening with a fraction of the structure ten times larger than the impactor's major diameter (a dimension sufficiently larger than the impacted area). After that, the fragmentation volume ( $F_v$ ) involved in the impact is computed (similarly as done in [27]), from the fragmentation level ( $F_l$ ):

$$\begin{aligned} F_l &= \frac{\epsilon_{tot}}{\delta} \\ F_v &= V \times F_l \end{aligned} \quad (1)$$

where  $\epsilon_{tot}$  is the impact total specific energy involved in the impact,  $\delta$  is the impact threshold for the catastrophic collision (e.g. 40 kJ/kg), and V is the volume of the part of the target involved in the impact. Fragment distribution is computed by combining both the approach used in CST [27] and IMPACT [3] models. The cumulative number of fragments is derived from the semi-empirical laws (such as those of Nishida [32], [31]), while the relation between the total number of fragments and their dimensions distribution is given by a 2D Voronoi pattern, constructed using as initial seed the semi-empirical laws. The single fragments are then considered ellipsoids with major axes the major dimension of the Voronoi polygons and as second and third axes equal between each other and computed iteratively to best match the total fragmentation volume obtained from the fragmentation level. The mass is redistributed per each fragment proportionally to the main size (computed with the Voronoi); while the velocity is defined using the approach defined in the IMPACT [3] model:

$$v_i = \sqrt{\frac{m_o}{m_i} v_o^2} \quad (2)$$

where equation 2 shows the way the velocity is distributed between the major bins ( $v_i$ ) of fragments after

the impact (of the impactor and target):  $m_o$  is the initial total mass involved in the collision,  $m_i$  is the mass of the single bin and  $v_o$  is the initial impact relative speed. While equation 3 computes the distribution of the velocities for each single fragment, where  $x$  is the ratio of the spread of velocity to the characteristic initial velocity:

$$f(x) = Ax^{\alpha-1}(1-x)^{\beta-1} \quad (3)$$

$f(x)$  is a beta function employed to redistribute the velocity between fragments.

Ultimately the distribution of the velocities in three dimensions is assumed spherically symmetric about the post-fragmentation ECI the velocity vector of the debris cloud's centre of mass, as done in the IMPACT model.

The macro analysis is not inspected in detail in this paper and no results are still not ready for a scientific publication. However, this second approach wants to estimate the breakup behaviour of solar power satellites when impacted by bigger structures (objects bigger than 1m in major dimensions and not just fragments), to capture the macro effects on the structures impacting and the eventual separation of major objects. Once the main substructure of the SPS impacted is selected (e.g. truss structure, panels, reflector), the fraction of this structure involved in the impact is selected as well for the macro-impact approach (using again the momentum balance). Then the object couple (impactor and target) is divided into macro components and the failure of major structural objects is inspected to verify if a certain energy threshold is exceeded for each of them, leading to separation. Together with this approach, a fragmentation model accounting for debris generation needs to be considered as well, and also in this case a semi-empirical model is employed but using an approach similar to the one used for the NASA SBM version of the ESA MASTER tool [35].

Once multiple scenarios have been run for the different impactors and target conditions (multiple structures and material types, as listed in the previous chapter), the fragmentation data are used as a dataset for the ML algorithm. The outcome of the training will be then employed inside the NESSY simulation at runtime to estimate the consequences of collisions together with the rest of the space environment.

## 5. LOCAL IMPACT ANALYSIS TEST CASES AND PRELIMINARY RESULTS.

The previously defined pipeline has been partially tested, and in this paper, some preliminary results are shown in more detail. This chapter shows two main use cases for the impact of small fragments in both LEO and GEO regimes. Table 4 shows the characteristics of the two test settings. The first test case (GEO-test) inspects the impact of an aluminium fragment against a support panel for a GEO SPS, and has been selected explicitly because

it can be easily validated through the Nishida experiments for the aluminium tests (data in [31]), to have a matter for comparison and validation of the fragments generation method. The second test instead inspects the collision of a small aluminium fragment against the LEO reflector membrane (the material considered is PEEK [12]). For both the two test cases the part of the pipeline which is involved in the analysis is the local fragmentation analysis, while the entire pipeline tests will be shown in the next publications.

Table 2. Test cases for the local breakup model analysis. ( $d$  = projectile diameter;  $t$  = plate thickness,  $v$  = initial speed orthogonal to the target main plane).

Test case	Parameter	Impactor	Target
GEO-test	Geometry	Sphere	Thin plate
	Material	Aluminium	PEEK
	Dimension	$d = 4 \text{ mm}$	$t = 3 \text{ cm}$
	Initial cond.	$v = 3.7 \text{ km/s}$	$v = 0 \text{ km/s}$
LEO-test	Geometry	Sphere	Thin plate
	Material	Aluminium	Aluminium
	Dimension	$d = 0.5\text{-}10 \text{ mm}$	$t = 10 \text{ }\mu\text{m}$
	Initial cond.	$v = 10 \text{ km/s}$	$v = 0 \text{ km/s}$

## 5.1. GEO test case

For the GEO test, the velocities considered are in the hypervelocity impact regime. Because of the dimension of the impactor this case is treated by the local analysis part of the pipeline. Firstly the momentum balance of the impact suggests that the collision will produce a breakup with a complete fragmentation of the impactor with a non-perforating impact (generation of a crater). Knowing the total kinetic energy involved in the impact, the fragmentation volume can be computed, and the Voronoi pattern is derived as described in the previous sections. Figure 7 shows the last iteration of the 2D Voronoi pattern generation process for the target (a similar one is also defined for the impactor), with highlighted just the polygons considered in the analysis domain (blue points correspond to the centroids of the polygons). Considering the major dimension of each fragment (polygon) the total actual fragmented volume is recovered as described in the previous chapter. The total number of fragments generated bigger than a certain dimension ( $a$ ) is plotted in Figure 8 (in blue), together with the empirical law (red) curve and the equivalent outcome from the NASA SBM (black). As expected the NASA SBM overestimates the number of the smallest and biggest fragments in the distribution. However, since this test case considers very small fragments and a relatively small range of fragment sizes, the SBM prediction is not that far. On the other side the semi-analytical approach shows a very good agree-

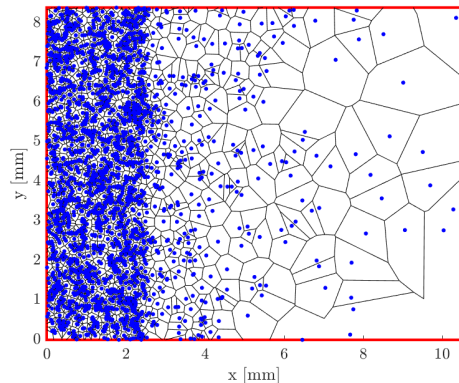


Figure 7. 2D Voronoi pattern generated from the estimate of the fragmentation volume for the target plate in the GEO test case.

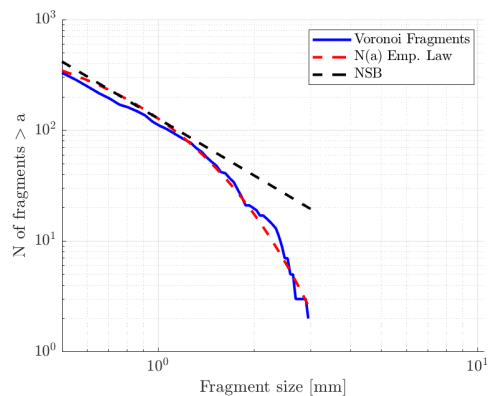


Figure 8. Total number of fragments bigger than a certain dimension ( $a$ ) for the GEO test case. Comparison between: Voronoi generated fragments (blue), experiment data regression curve from Nishida [31] (red) and the empirical law of the NASA SBM (black). Fragments up to 0.5mm minimum dimension.

ment with the empirical data.

Figure 9 reports the results of the mass and velocity allocation for the different fragments from the semi-empirical model (SE) compared with the NASA SBM sampling (in red). It is clear from the plot the stochastic allocation of both mass and velocity in the case of the NASA SBM. The mass allocation from the semi-empirical model is directly correlated to the dimension and is also lower than the estimate from the NASA SBM average one, especially for small fragment dimensions. For the velocity instead, the SE estimate values are slightly higher. Table 3 instead shows the different estimates of total mass and fragmentation volume as computed with the momentum balance and the outcome of the semi-empirical model developed, compared with the experimental data from Nishida. It is possible to notice that the semi-empirical approach estimate remains sufficiently close to the actual value after the definition of the Voronoi pattern.

Table 3. Total fragmentation volume and mass estimated via the semi-analytical method (SA) and initial momentum balance (MB), compared comparison with experimental data from Nishida (collection accuracy 73%).

	Nishida	MB estimate	SA approach estimate
Tot. fr. volume ( $cm^3$ )	0.064	0.068	0.066
Tot. fr. mass ( $mg$ )	173	183	178

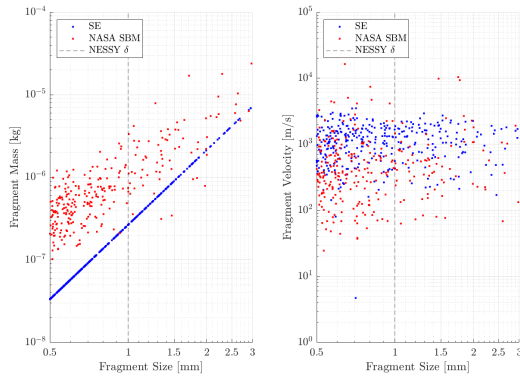


Figure 9. Fragments mass (on the left) and velocity (on the right) distributions for the GEO test. Comparison between the fragments generated with the semi-empirical approach and the NASA SBM. The black dashed line represents the minimum fragment dimension considered in NESSY simulation ( $\delta$ ).

## 5.2. LEO test case

The LEO test case instead considers the impact of a spherical aluminium fragment against the LEO reflector membrane. As indicated in Table 4, the thickness of the membrane is extremely small (about  $10 \mu m$ ), resulting in a very small thickness-to-impactor diameter ratio. At present, there are no specific studies focused on a precise assessment of the perforation dynamics of the LEO reflector membrane. Few studies (e.g. [12] and [26]) provide pertinent analyses for this scenario. However, as investigated by the literature, for very thin plates under hypervelocity impact the target is usually perforated, even with impactor diameters significantly smaller than those relevant to this investigation. Considering this second use case with the semi-empirical pipeline, it is interesting to consider different scenarios varying the diameter of the impactor to understand after which critical diameter the impacting object will pass through the membrane almost undamaged. Considering the first step of the pipeline, the momentum balance (comparison of the total kinetic energy with the breakup energy threshold) suggests a non-catastrophic breakup of the impactor at about  $9 mm$  in diameter for the spherical aluminium projectile. For this use case, the fragments generated from the plates are completely pulverized, but those coming from the projectile are bigger than the NESSY thresh-

old. However, it is interesting to verify through a more precise investigation which is the critical diameter leading to a perforation of the membrane not breaking up. To do so a series of numerical simulations have been set up, using the ANSYS Autodyn environment. The simulation is set up using a 2D axis-symmetric Smoothed Particle Hydrodynamics (SPH) solver. A similar setting has been widely employed in literature for hypervelocity impact simulation (e.g. [17], [24]). Figure 10 shows the initial configuration in axisymmetric configuration, with the impactor and membrane filled with SPH particles of the two different material models. Initial velocity is imposed on the projectile in the  $X$  direction, while the plate is fixed at the boundaries. The dimension of the plate in  $Y$  direction is computed as 6 times higher than the radius of the projectile, to make sure this does not influence in any way the simulation results. To let the dynamic fully develop the simulation has been run for  $10^{-2} ms$ . The diameters considered for the impactor are the following: 10, 7, 5, 3, 2 and 1 mm. The rest of the main high-level characteristics of the simulation settings are indicated in Table 4. Figure 10 shows that at the end of the simulation the case of diameter 10 mm shows material bulk failure (in red) just for a few particles already detached from the main body, superficial damage and in general plastic deformation mainly on the backside. Bulk failure in ANSYS-Autodyn refers to the material's loss of structural integrity due to excessive deformation or stress, typically leading to disintegration. It occurs when the material exceeds its strain failure criteria. The test with a diameter 7 mm instead shows a larger portion with bulk failure and detachment of material. The other test cases report a large breakup of the projectile or major failure. Between 3 and 5 mm the projectile seems as well to partially fracture and probably later go through a progressive mass reduction. This experiment proves that the critical perforating diameter is larger than 7 mm and probably around 10 mm (as in agreement with the momentum balance outcome). However, impactor diameters up to 7 mm cause the breakup of the projectile, producing fragments that could also be still bigger than 1 mm.

## 6. CONCLUSIONS AND NEXT STEPS

This paper presents a tailored approach for modelling collision and fragmentation events related to Solar Power Satellites, with applicability to other large space structures. The proposed pipeline enables the simulation of

Table 4. ANSYS-Autodyn simulation setting for the LEO test case.  $X$  indicates the number of SPH particles in the  $x$ -symmetry direction. More details about PEEK material in [12].

Object	Parameter	Setting
Membrane	Shape	thin plate
	Material	PEEK AptivTM
	EOS	Polynomial
	Strength	Steinberg Guinan
	Failure model	Johnson Cook
	Erosion	-
	SPH objects (X)	4
	Initial condition	Clumped
Impactor	Shape	Sphere
	Material	Aluminium 2024
	EOS	Polynomial
	Strength	Steinberg Guinan
	Failure model	Johnson Cook
	Erosion	-
	SPH objects (X)	400 - 40 000
	Initial condition	X velocity

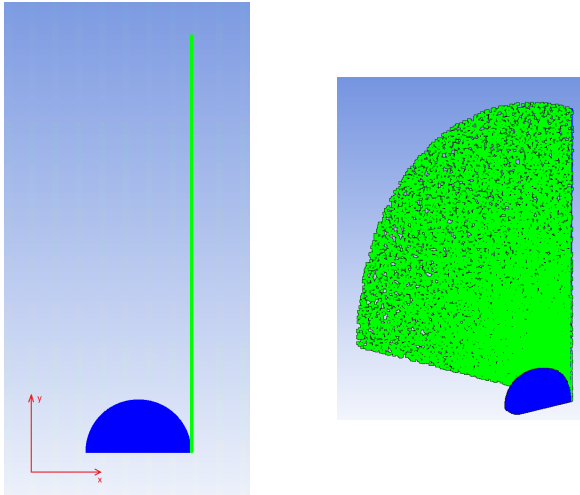


Figure 10. Initial simulation setting in ANSYS-Autodyn using SPH modelling in axisymmetric mode: on the left the symmetric  $x$ -direction view and on the right a lateral view of the rotated  $x$ -symmetric geometry. In blue the impactor sphere and in green the plate.

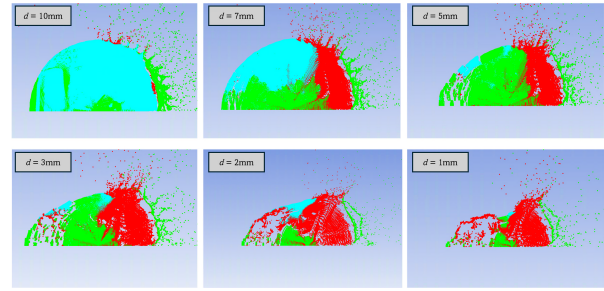


Figure 11. Analysis of the critical impactor diameter for the LEO reflector membrane (simulation in ANSYS-Autodyn 2024). Visualization of different diameter scenarios  $10^{-2}$  ms after the contact of the projectile with the membrane. The different colours define the status of the material at that time instant: red = bulk failure, cyan = plastic deformation, green = elastic deformation, blue = hydro deformation.

collision effects using a semi-empirical model, accounting for both local impacts and big catastrophic impacts. At this stage, only part of the pipeline has been extensively tested, and preliminary results are presented for a few simple scenarios. The final pipeline will be designed for integration into an evolutionary algorithm such as NESSY, enabling an optimal long-term assessment of the presence of SPS in the space environment. Preliminary results show good accordance with experimental data. Besides the tests of the pipeline regarding local fragmentation in GEO, the paper reports also a parametric study conducted through ANSYS-Autodyn environment about the impact on the LEO reflector membrane. The main next steps regard the finalization of the macro analysis part of the pipeline, allowing the simulation of impacts between large structures and the SPSs. Furthermore, the final next step will be testing and validating the ML-based algorithm generalization.

## ACKNOWLEDGMENTS

This work is partially supported by the ESA-funded project SOLERO - Solar Power Satellite vs the Space Environment, Co-Sponsored Research Agreement No. 4000144200/24/NL/MGu/my.

## REFERENCES

1. Y. Wanf, C. Wilson, M. Vasile, *Multi-layer temporal network model of the space environment*, Proceedings of the American Astronautical Society Meeting 2023, available at: [link](#)
2. E. Ausay, A. G. Cornejo, C. D. Boyle, B. T. Blake, T. Sato, A. Horn, K. Palma, F. Pistella, N. Todd, J. Zimmerman, N. Fitz-Coy, J.-C. Liou, M. Sorge, T. Huynh, J. Opiela, P. H. Krisko, H. Cowardin, and M. Rivero, *A Comparison of the SOCIT and Debrisat*

- Experiments*, Proceedings of the ESA Space Debris Conference, 2017, available at: [ESA proceedings link](#)
3. M. Deanna, S. Marlon, *The IMPACT Satellite Fragmentation Model*, Acta Astronautica, vol. 195, pp. 547-555, June 2022, available at: [link](#)
  4. J. Murray, H. Cowardin, *Analysis of the DebrisSat Fragments and Comparison to the NASA Standard Satellite Breakup Model*, First International Orbital Debris Conference, 2019, available at: [NASA link](#)
  5. P.N. Verma, K.D. Dhote, *Characterising Primary Fragment in Debris Cloud Formed by Hypervelocity Impact of Spherical Stainless Steel Projectile on Thin Steel Plate*, International Journal of Impact Engineering, col 120, pp. 118-125, Oct 2018, available at: [link](#)
  6. A. Fikes, E. Gdoutos, M. Klezenberg, A. Ayling, O. Mizrahi, J. Sauder, C. Sommer, A. Truong, A. Wen, A. Wu, R. Madonna, H. Atwater, A. Hajimiri, S. Pellegrino, *The Caltech Space Solar Power Demonstration One Mission*, IEEE, 2022, available at: [link](#)
  7. J. C. Mankins, *SPS-Alpha: The First Practical Solar Power Satellite via Arbitrarily Large Phased Array*, 10th International Energy Conversion Engineering Conference, 2012, available at: [link](#)
  8. ESA Space Debris Office, *DISCOSweb*, European Space Agency, available at: [ESA website \(accessed Dec 2024\)](#).
  9. N. L. Johnson, P. H. Krisko, J.-C. Liou, P. D. Anz-Meador, (2001), *NASA's new breakup model of evolve 4.0*, Advances in Space Research, vol. 28, no. 9, pp. 1377-1384, 2001, available at: [link](#)
  10. S. White, F. Sabri, R. Flytkjaer, *Study on Cost-Benefit Analysis of Space-Based Solar Power (SBSP) Generation for Terrestrial Energy Needs - Final Report*, Frazer-Nash Consultancy Limited, 2022
  11. I. Cash, et al, *CASSIOPEIA solar power satellite*, IEEE International Conference on Wireless for Space and Extreme Environments (WiSEE), 2017, available at: [DOI link](#).
  12. SBSP Team Thales Alenia Space, *Pre-phase a system study of a commercial-scale space-based solar power (SBSP) system for terrestrial needs*, 2023.
  13. A. D'Ambrosio, S. Servadio, P. M. Siew, R. Linares, *Novel Source-Sink Model for Space Environment Evolution with Orbit Capacity Assessment*, AAS/AIAA Astrodynamics Specialist Conference, 2022, available at [link](#)
  14. ESA Space Debris Office, *ESA'S annual space environment report - 2024*, European Spcae Agency, 2024, available at: [ESA link](#)
  15. M. Murray, P Anz - Meador, H. Cowardin, M. Heather, *Analysis of hypervelocity-impacted thin films for space applications*, International Journal of Impact Engineering, vol. 180, Article 104709, Oct 2023, available at [link](#)
  16. L.S. Alesbrook, M.J. Burchell, C.T. Cornwell, R. Corsaro, F. Giovane, J.C. Liou, J. Tandy, P.J. Wozniakiewicz, *Hypervelocity impact induced light flash experiments on single and dual layer Kapton targets to develop a time of flight space dust and debris detector*, International Journal of Impact Engineering, Vol 187, May 2024, available at: [link](#)
  17. C. Ryan, *Momentum Transfer due to Hypervelocity Impacts into Spacecraft Solar Arrays*, TU-Delft thesis, 2021, available at: [thesis link](#)
  18. M.V. Silnikov, I.V. Guk, A.F. Nechunaev, N.N. Smirnov, *Numerical simulation of hypervelocity impact problem for spacecraft shielding elements*, Acta Astronautica Vol 150, Sept 2018, pp. 56-62, available at: [DOI link](#)
  19. N. Cimmino, G. Isoletta, R. Opromolla, G. Fasano, A. Basile, A. Romano, M. Peroni, A. Panico and A. Cecchini, *Tuning of NASA Standard Breakup Model for Fragmentation Events Modelling*, New Space: Advances in Space Science and Engineering, Vol 8, 2021, available at: [DOI link](#)
  20. Y. Wang, P. De Marchi, M. Vasile, *A Stochastic Dynamic Network Model of the Space Environment*, Advances in Space Research, 2024, available at [Arxiv link](#)
  21. P. De Marchi, Y. Wang, and M. Vasile, *Space Environment Impact of Solar Power Satellites*, AAS 25-344, preprint, 2025, available at: [AAS conference proc.](#)
  22. A.J. Piekutowski, J. Andrew, *Characteristics of debris clouds produced by hypervelocity impact of aluminium spheres with thin aluminum plates*, International Journal of Impact Engineering Vol 14, 1993, pp. 573-586, available at [DOI link](#)
  23. L. Stein, *LEO SATCOM Report*, Mar. 2022, available at: [SATCOM link](#)
  24. X. Zhang, G. JIA, H. HUANG, *Fragment Identification and Statistics Method of Hypervelocity Impact SPH Simulation*, Chinese Journal of Aeronautics, 2011, available at: [DOI link](#)
  25. A. Rossi, P. Farinella, *Collision rates and impact velocities for bodies in low Earth orbit*, ESA Journal, vol. 16, no. 3, pp. 339-348, 1992, available at [DOI link](#)
  26. L. Visagie, V. Lappas, Sven Erb, *Drag sails for space debris mitigation*, 2015, available at [DOI link](#)
  27. A. Francesconi, C. Giacomuzzo, L. Olivieri, G. Sarego, M. Duzzi, F. Feltrin, A. Valmorbidia, et al, *CST: A new semi-empirical tool for simulating spacecraft collisions in orbit*, Acta Astronautica Vol. 160, July 2019, pp. 195-205, available at [link](#)
  28. R. Gordon, C. McInnes, *End-of-life considerations for orbital solar reflectors*, AAS/AIAA Space Flight Mechanics Meeting, 2025, available at [link](#)
  29. M. Lambert, *Hypervelocity impacts and damage laws*, Advances in Space Research Vol. 19, Issue 2, 1997, pp. 369-378, available at: [link](#)

30. J. Arnold, E. Christiansen, A. Davis, J. Hyde, et al, *NASA Handbook MMOD design*, 2009, Johnson Space centre Publications, available at: [link](#)
31. M. Nishida, Y. Hiraiwa, K. Hayashi, S. Hasegawa, *Scaling laws for size distribution of fragments resulting from hypervelocity impacts of aluminum alloy spherical projectiles on thick aluminum alloy targets: Effects of impact velocity and projectile diameter*, International Journal of Impact Engineering Vol 109, Nov 2017, pp. 400-407, available at: [link](#)
32. M. Nishida, Y. Hiraiwa, K. Hayashi, S. Hasegawa, *Ejecta Size Distribution Resulting from Hypervelocity Impact of Spherical Projectiles on CFRP Laminates*, Procedia Engineering, Vol. 58, 2013, pp. 533-542, available at: [link](#)
33. D. McKnight, L. Nagl, R. Maher, *Fragmentation Algorithms for Strategic and Theater Targets (FASTT) Empirical Breakup Model*, 1993, DNA-TR-94-104
34. K. Nakashima, T. Hanada, Y. Akahoshi, T. Harano, Y. Machida, and S. Fukushige, *Low-Velocity Catastrophic Impact on Micro Satellite*, Proceedings of the Fourth European Conference on Space Debris, 2005, available at: [link](#)
35. R. L. Andrişan, A. G. Ioniță, R. D. González, N. S. Ortiz, F. P. Caballero, and H. Krag, *Fragmentation event model and assessment tool (FREMAT) supporting on-orbit fragmentation analysis*, in Proceedings of the ESA Space Debris Conference, 2017
36. C. Mankins, *SPS-ALPHA: The First Practical Solar Power Satellite via Arbitrarily Large Phased Array*, NASA NIAC Phase 1 Project, Sep. 15, 2012, available at: [link](#)
37. O. Çelik, C. McInnes, *A Constellation Design for Orbiting Solar Reflectors to Enhance Terrestrial Solar Energy*, Acta Astronautica Vol. 217, April 2024, pp. 145-161, available at: [link](#)
38. O. Çelik, A. Viale, T. Oderinwale, L. Sulbhewar, C.R. McInnes, *Enhancing Terrestrial Solar Power Using Orbiting Solar Reflectors*, Acta Astronautica Vol. 195, June 2022, pp. 276-286, available at: [link](#)
39. X. Li, B. Duan, L. Song, Y. Yang, Y. Zhang, W. Yiqun, D. Wang, *A New Concept of Space Solar Power Satellite*, Acta Astronautica Vol. 136, July 2017, pp. 182-189, available at: [link](#)